AIAA JOURNAL
Vol. 36, No. 3, March 1998

Competing Mechanisms of Compressible Dynamic Stall

M. S. Chandrasekhara*
U.S. Naval Postgraduate School, Monterey, California 93943
M. C. Wilder†
MCAT Inc., Mountain View, California 94043
and
L. W. Carr‡
NASA Ames Research Center, Moffett Field, California 94035-1000

Earlier experiments have documented the onset of compressible dynamic stall either from the bursting of a leading-edge laminar separation bubble or from a leading-edge shock, depending on the Reynolds number and Mach number. For certain combinations of conditions, the supersonic flow and the bubble dynamics compete with each other. The consequent complex interactions lead to a newly discovered mechanism of dynamic stall onset. Details of these various mechanisms are discussed.

Nomenclature

C_p = pressure coefficient
$C_{P\min}$ = peak suction pressure coefficient
c = airfoil chord
f = frequency of oscillation, Hz
k = reduced frequency, $\pi fc/U_\infty$
M = freestream Mach number
Re = Reynolds number based on chord
U_∞ = freestream velocity
x, y = chordwise and vertical distance
α = angle of attack
α_m = amplitude of oscillation
α_0 = mean angle of attack
ω = circular frequency, rad/s

I. Introduction

IN earlier studies of compressible dynamic stall over a NACA 0012 oscillating airfoil, it was established that dynamic stall occurred from the bursting of a laminar separation bubble that formed near the airfoil leading edge as the airfoil was pitched up.[1] The bursting correlated well with a maximum value of the leading-edge adverse pressure gradient following the suction peak being reached for each freestream Mach number.[2] These tests were carried out for Mach numbers of 0.2–0.45 at Reynolds numbers ranging from 0.36×10^6 to 0.81×10^6 where a laminar separation bubble always formed. Interferograms of the dynamic stall flow at $M = 0.45$ showed that multiple shocks formed over the airfoil,[3] which, however, did not seem to play a major role in initiating dynamic stall. Because no flow separation was observed due to the shocks, it was deduced that the pressure rise across the shocks was less than 1.4, the minimum pressure jump needed to induce flow separation.[4] This result was supported by a fringe count that yielded a maximum local Mach number of about 1.13. Interestingly, the leading-edge adverse pressure gradient was found to be nearly constant[2] and very low when dynamic stall was initiated. Studies over a tripped airfoil showed that tripping completely eliminated the bubble and that dynamic stall occurred as the leading-edge adverse pressure gradient exceeded a (higher) maximum value.[5] Once again, multiple shocks were present in the $M = 0.45$ flow, but dynamic stall onset could be correlated with a considerably larger adverse pressure gradient when compared with the untripped airfoil flow. Regardless, the critical nondimensional adverse pressure gradient at onset of dynamic stall decreased with increasing Mach number, leading to the conclusion that compressibility effects reduced the ability of the airfoil boundary layer to withstand the forces causing unsteady separation. Further, it was found that this critical adverse pressure gradient was reached at progressively lower angles of attack, confirming results of earlier schlieren studies[3] that showed compressibility caused premature dynamic stall onset. This result is in direct contrast to that of the computational studies at a Reynolds number of about 1×10^5 by Sankar and Tassa[6] and Choudhuri and Knight,[7] who found a delay of dynamic stall with increasing Mach number. Thus, it is clear that the understanding of the details of the dynamic stall onset and its subsequent development is still far from complete.

In view of the relevance of the problem to helicopters that operate at higher Reynolds numbers, a better understanding of the flow physics and effects of Reynolds number and Mach number is needed. With this in mind, studies were recently conducted on an oscillating airfoil with a 6-in. chord, providing data at Reynolds numbers twice those of the earlier studies for each freestream Mach number. By properly tripping the airfoil,[8] an effective Reynolds number of about 4×10^6 has been simulated as determined by comparison of the airfoil pressure distributions with the well-known data of McCroskey et al.[9]

Interestingly, even at the higher Reynolds number, dynamic stall over the untripped airfoil occurred from the laminar separation bubble bursting at $M = 0.3$; at $M = 0.45$, shock-induced separation led to dynamic stall. Tripping this larger airfoil eliminated the bubble, and it was found that dynamic stall was initiated from the strong adverse pressure gradient at $M = 0.3$ and from a shock at $M = 0.45$ (Ref. 8). The details of the flow development for each Mach number of the experiment appeared to be different, however. In particular, the development of the local supersonic region and its complex interactions with the bubble or the boundary layer seemed to dictate the further events in the flow. This paper focuses on the details of these various mechanisms and interactions.

II. Experimental Facility and Technique

The experiments were carried out in the compressible dynamic stall facility (CDSF) located in the Fluid Mechanics Laboratory of NASA Ames Research Center. The CDSF is an in-draft wind tunnel with a 25 × 35 cm test section and is equipped with an airfoil oscillating drive mechanism to produce a sinusoidal variation of

Presented as Paper 96-1953 at the AIAA 27th Fluid Dynamics Conference, New Orleans, LA, June 17–20, 1996; received Jan. 29, 1997; revision received Sept. 25, 1997; accepted for publication Oct. 21, 1997.

*Associate Director and Research Professor, Navy–NASA Joint Institute of Aeronautics, Department of Aeronautics and Astronautics; mailing address: M.S. 260-1, NASA Ames Research Center, Moffett Field, CA 94035. Associate Fellow AIAA.

†Senior Research Scientist, Navy–NASA Joint Institute of Aeronautics. Member AIAA.

‡Research Scientist and Group Leader, Unsteady Viscous Flows, Aeroflightdynamics Directorate, Aviation Research, Development and Engineering Center, U.S. Army ATCOM, and Fluid Mechanics Laboratory Branch. Member AIAA.

angle of attack. Mean angles of attack of up to 15 deg and maximum amplitude and oscillation frequency of 10 deg and 100 Hz, respectively, are possible. The tunnel flow (maximum freestream Mach number of 0.5) is produced by a 240,000 ft^3/min, 9000-hp compressor and is controlled by a variable area downstream choked throat. Additional details can be found in Ref. 10. For the lower-Reynolds-number experiments, a 3-in. chord NACA 0012 airfoil was supported between two 15-cm-diam glass windows by small pins permitting full flowfield visibility. For the higher-Reynolds-number tests, a 6-in. chord NACA 0012 airfoil was supported between metal ports with L-shaped optical glass inserts permitting visibility over the first 35% of airfoil chord. The larger airfoil was also instrumented with pressure taps.

The experimental data were obtained using the recently developed real-time technique of point diffraction interferometry (PDI). It uses an expanded laser beam to fill the entire field of view in a standard Z-type schlieren configuration, with the optics aligned to minimize astigmatism. A predeveloped, partially transmitting photographic plate replaces the knife edge. In operation, with no flow in the test section, a pinhole is created in situ in the photographic plate to serve as a point diffractor. The light beam passing through the test section is phase shifted and deflected from its parallel path by the density changes in the flow and thus focuses to a bigger spot around the pinhole. The portion of this light passing through the pinhole then becomes the reference beam and interferes with that passing around it (signal beam) to create fringes in real time, which are captured on Polaroid film. The image magnification was varied suitably and interferograms were obtained for two values of the magnification, viz. ≈ 2 and 10.

The experimental conditions for the present study were $M = 0.2$, 0.3, 0.35, 0.4, and 0.45 and $k = 0$ (steady flow), 0.025, 0.05, 0.075, and 0.1; the angle of attack was varied as $\alpha = (10 \text{ deg} + 10 \text{ deg} \sin \omega t)$. The Reynolds number was 0.54×10^6 for the 3-in. model and 1.1×10^6 for the 6-in. airfoil at $M = 0.3$. The interferograms were obtained for both untripped and tripped airfoils. The boundary-layer trip on the 3-in. airfoil consisted of a distributed roughness, about 70 μm in height and located across $0.01 \leq x/c \leq 0.03$ and is fully described in Ref. 5. That on the 6-in. airfoil was a 1.5%-chord long, serrated leading-edge address label, about 75 μm thick, glued spanwise over the airfoil between $x/c = 0.015$ and 0.03.

The estimated uncertainties in the data are as follows:

Mach number	± 0.005
angle of attack	0.05 deg
reduced frequency	0.005
C_p	± 0.1 at $M = 0.3$
$C_{p_{\min}}$	-0.5 at $M = 0.3$
	-0.35 at $M = 0.45$
$[dC_p/d(x/c)]$	± 25

The uncertainty in C_p depends on the fringe number under consideration and is one fringe for the flow in general with about three fringes possibly undetectable near the suction peak for the 3-in. airfoil and about seven fringes undetectable for the 6-in. airfoil at $M = 0.3$. Because the correction for solid and wake blockage as determined from the procedure described in Ref. 11 was less than 5% for $C_p = -6.0$ at $M = 0.3$, no corrections were applied to the measured and PDI-derived pressures.

III. Results and Discussion

A. Leading-Edge Flow Development

Figure 1 summarizes the peak suction at different angles of attack for freestream Mach numbers of 0.3, 0.35, 0.4, and 0.45 at $k = 0.05$ for the 3- and 6-in. airfoils tested in the study. Both untripped and tripped airfoil data are included. The critical pressure coefficient at each Mach number is also indicated. For $M = 0.3$, the flow over both the 3- and the 6-in. untripped airfoils is subsonic. For the tripped 6-in. airfoil at 14 deg, a region of slightly supersonic flow is observed. However, the fringe pattern in this case indicated that this was only near the suction peak region, and hence no influence was felt on the dynamic stall process that was already under way.

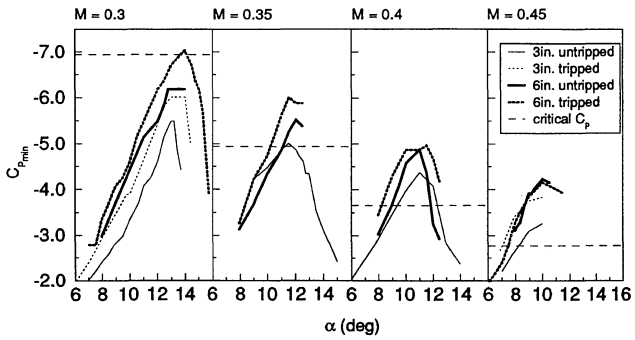

Fig. 1 Peak suction development at $k = 0.05$ for different Mach numbers and airfoils.

For $M = 0.35$, the flow over the 3-in. untripped airfoil barely becomes supersonic and thus, as expected, is similar to that over the 6-in. tripped airfoil at $M = 0.3$. The peak suction at $M = 0.35$ for the 6-in. airfoil exceeds the critical value for both the untripped and tripped cases. As can be expected, the supersonic velocities are higher for the tripped case because tripping effectively produces a higher Reynolds number condition, where viscous/inviscid interactions are reduced. The angle of attack at which supersonic flow first appears is around 10 deg for the tripped flow and about 11 deg for the untripped case, both of which are still less than the dynamic stall onset angle. The maximum local Mach number is in the range of 1.05–1.1 for both cases.

The results for $M = 0.45$ show that the critical pressure coefficient, $C_p = -2.76$, is reached at very low angles of attack, about 7 deg for the 6-in. airfoil and 8 deg for the 3-in. airfoil. The data for the 3-in. untripped airfoil at $M = 0.45$ show a trend that is more consistent with that observed for the 6-in. airfoil at $M = 0.35$ because the Mach number at the peak suction value is about 1.1. The data for the 3-in. tripped airfoil are similar to those for the 6-in. airfoil, but for the latter the maximum C_p attained far exceeds the critical value for both the untripped and tripped cases. In these flows, the local Mach number of about 1.35 is large enough to produce strong shocks that can induce flow separation. Consequently, the details of the dynamic stall process are also expected to be different.

If the flow remains subsonic during the pitch-up motion of the airfoil, dynamic stall occurs either from the bursting of a laminar separation bubble due to a large positive pressure gradient or at higher (equivalent) Reynolds numbers, simply from the strong adverse pressure gradient following the suction peak. However, when the flow becomes supersonic, the onset mechanism is different, depending upon the formation of shocks and their strength. If strong shocks form (upstream local Mach number ≥ 1.2), shock-induced separation can occur. If the shocks are weaker, the supersonic flow and the bubble can grow independently or interact strongly, depending upon the flow conditions, thus introducing a new mechanism of dynamic stall onset.

B. Laminar Separation Bubble Induced Dynamic Stall Onset

The adverse pressure gradient near the leading edge of an airfoil obviously plays a major role in its stall behavior, especially because compressible dynamic stall is a leading-edge type of stall at all Reynolds numbers. At low Reynolds numbers, the laminar boundary layer on the upper surface separates initially at very low values of adverse pressure gradient and reattaches after transitioning to turbulent flow, thus forming a laminar separation bubble. If the airfoil flow is tripped, or the Reynolds number is sufficiently high, a turbulent boundary layer develops that ultimately separates due to high adverse pressure gradient. The onset of dynamic stall from bubble bursting is discussed later. The differences in the flow details when the airfoil was tripped are also noted.

Figure 2 presents some point diffraction interferograms at different angles of attack for a Mach number of 0.3 and a reduced frequency of 0.05 for the 6-in. untripped airfoil. As is well known,[1] the fringes in the images represent contours of constant density. The stagnation point is enclosed by the nearly semicircular fringe on the lower surface. As the flow accelerates from this point, more fringes

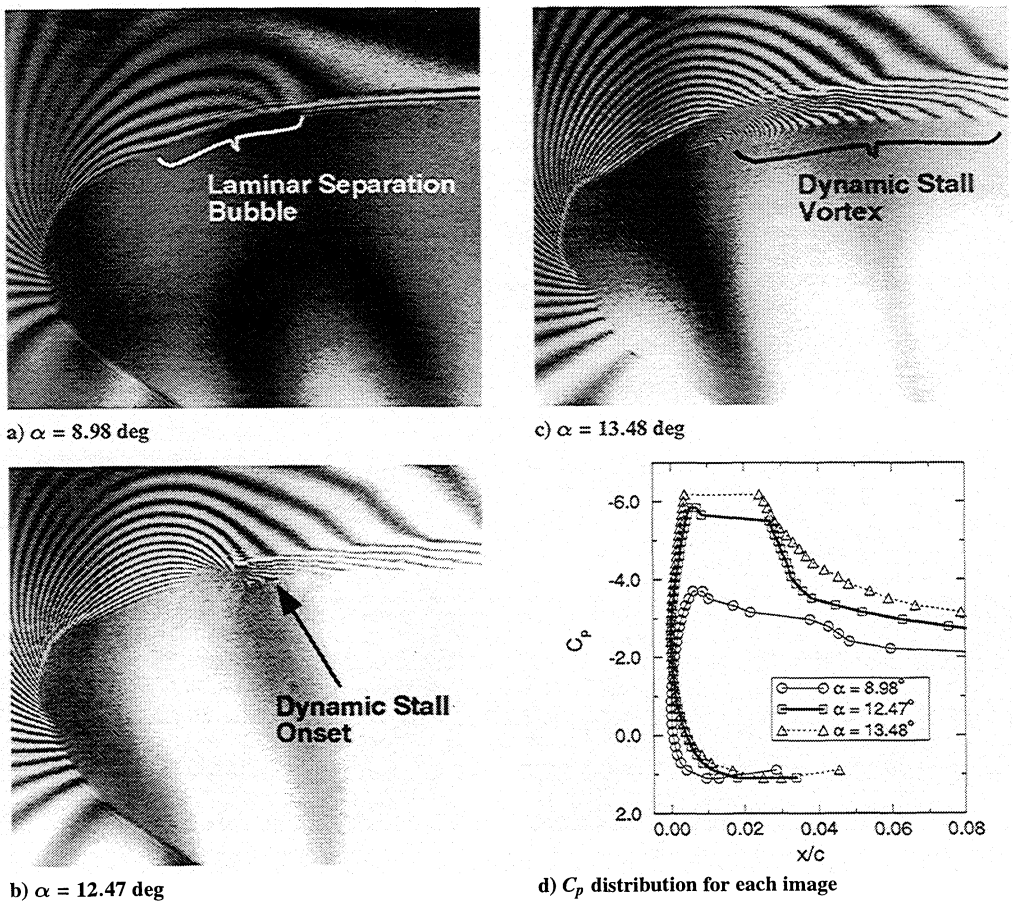

a) α = 8.98 deg

c) α = 13.48 deg

b) α = 12.47 deg

d) C_p distribution for each image

Fig. 2 PDI images illustrating laminar separation bubble induced dynamic stall at M = 0.3 and k = 0.05 for the untripped 6-in. chord airfoil.

develop, and the last fringe to close on itself near the leading edge on the upper surface marks the suction peak. In Fig. 2a, the flow for an instantaneous angle of attack of 8.98 deg is shown. In it, some fringes downstream of and close to the suction peak become locally parallel to the airfoil surface between $x/c = 0.025$–0.04. It has been shown in Ref. 1 that such a pattern corresponds to a laminar separation bubble. The bubble seen in Fig. 2a is smaller than that obtained for the 3-in. airfoil described in Ref. 1 due to the higher Reynolds number of the 6-in. chord airfoil flow. Figure 2b shows dynamic stall onset at $\alpha = 12.47$ deg being caused by the bursting of the bubble. At this condition, vertical fringes appear near the downstream end of the bubble in the boundary layer. These vertical fringes are the first evidence that dynamic stall has started.[1] A further increase in angle of attack causes the dynamic stall vortex to grow as shown in Fig. 2c. The density values corresponding to each fringe seen in the images can be converted to static pressures under isentropic flow assumptions.[1] Figure 2d shows the pressure distributions for images in Figs. 2a–2c obtained using this method. The onset of dynamic stall can be seen in these graphs as the flattening of the pressure distributions near the downstream end of the bubble as it bursts and the dynamic stall vortex forms. The flat region extends farther over the upper surface as the vortex grows. The airfoil suction may continue to increase until the separation point reaches the leading edge and then begin to drop. The highest local Mach number reached for this case was about 0.94, at an angle of attack of about 12.47 deg. Thus, both the PDI images and the pressure distributions clearly show that the dynamic stall process begins with the bursting of the separation bubble.

The adverse pressure gradients in the flow as determined by a least-squares fit from the suction peak to the beginning of the plateau in the pressure distributions are presented in Fig. 3. For the tripped airfoil, the first six (or if fewer were present, as many available) fringes immediately downstream of the suction peak were used for the line fit. Figure 3 shows that the adverse pressure gradient increases steadily with angle of attack to a value of about 175. Depending upon the local flow dynamics, such as the state of the turbulence in the shear layer enveloping the vortex,[5] the level is constant

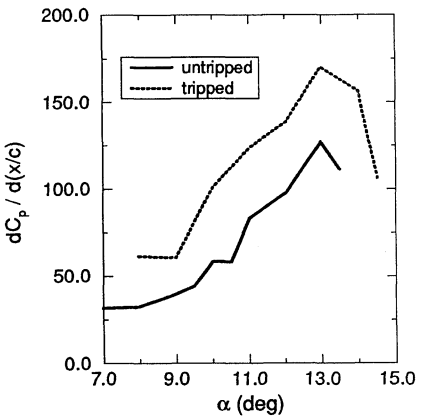

Fig. 3 Adverse pressure gradient development for oscillating 6-in. chord airfoil: M = 0.3 and k = 0.05.

during a very small angle of attack range when the vortex organizes and then drops as it begins to convect.

PDI pictures taken during the test show that bubble bursting was also the cause of dynamic stall at $M = 0.3$ and 0.35 for all reduced frequencies studied for the 3-in. airfoil. Only marginal differences were noticed in the adverse pressure gradient value at stall onset.

As stated earlier, the airfoil was tripped to eliminate the bubble and to study the onset of dynamic stall in fully turbulent flow. Removal of the bubble eliminates one major factor in the flow development by reducing the problem to one dominated only by the local adverse pressure gradient. It is clear from Fig. 3 that the nondimensional adverse pressure gradients over the tripped airfoil are larger than those over the untripped airfoil for all angles, despite the small loss of the boundary-layer momentum due to the presence of the trip. Ultimately, once dynamic stall ensues, the peak adverse pressure gradient begins to fall along with the peak suction. This result appears to be valid also for cases where tripping resulted in higher suction peaks, causing mildly supersonic velocities and weak shocks.

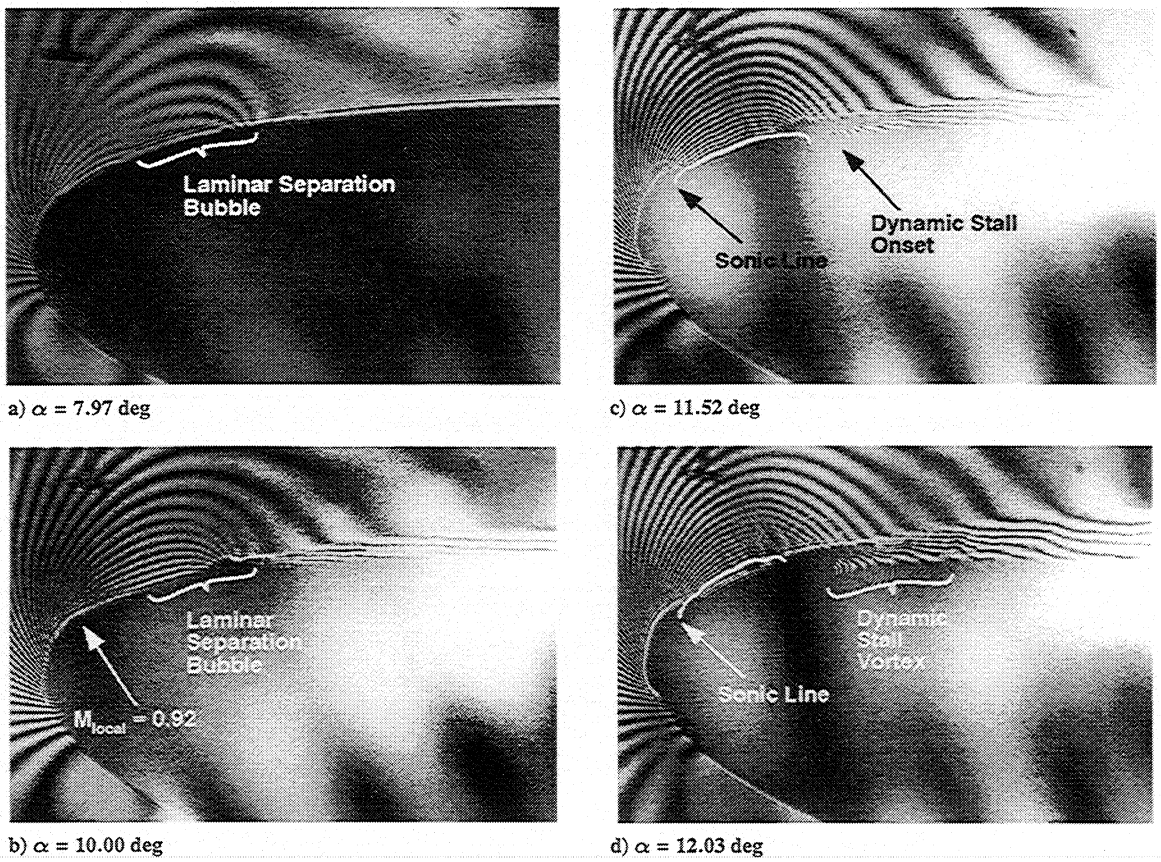

Fig. 4 PDI images illustrating dynamic stall onset from interactions of laminar bubble and locally supersonic flow at $M = 0.35$ and $k = 0.05$ for the untripped 6-in. chord airfoil.

C. Dynamic Stall Onset from Interactions of Laminar Bubble and Supersonic Flow

As explained during discussions of Fig. 1, the local flow over the untripped airfoil attains supersonic velocities as the freestream Mach number is increased. However, this usually occurs after the laminar separation bubble has formed. The growth of the supersonic flow region and the tendency of the bubble to burst with increasing angle of attack present a situation when complex interactions occur, leading to a new source of dynamic stall.

Figure 4a shows a PDI image for an angle of attack of 7.97 deg for $M = 0.35$ and $k = 0.05$ for the 6-in. untripped airfoil. As before, a laminar separation bubble can be seen in the picture; it ends where the fringes near the leading edge turn abruptly toward the airfoil surface (at $x/c \approx 0.04$). The boundary layer downstream of the bubble is still fairly thin. In Fig. 4b, at an angle of attack of 10.00 deg, the boundary layer begins to thicken at the downstream end of the bubble. The Mach number corresponding to the peak suction pressure now is about 0.92. Soon after, the local flow becomes supersonic. At this instant, the suction peak flow is supersonic, but the bubble is subsonic, and the two are separated by some distance. The supersonic region grows more along the airfoil than above it and extends to the bubble by $\alpha = 11.5$ deg (Fig. 4c). A close examination of the local fringe pattern indicates that the fringe denoting the suction peak is absent. Instead, the fringes develop parallel to the airfoil upper surface. The nearly flat fringes imply that the adverse pressure gradient is significantly reduced (Fig. 5) from that observed for the case of $M = 0.3$ and $k = 0.05$ where the flow is subsonic. It should be noted that although the bubble flow is subsonic everywhere, its upstream end is suddenly subjected to a supersonic flow. At this time the boundary layer at the downstream end of the bubble becomes even thicker (a precursor to stall). At the same time, tiny disturbance waves form in the supersonic flow region as the Mach number at the suction peak reaches about 1.05 (also see Fig. 6). These are believed to be expansion and compression waves reflecting off the sonic line above the convex leading edge of the airfoil and the shear layer. Guderley[12] has shown that multiple reflections are possible in transonic potential flow over a convex curved surface

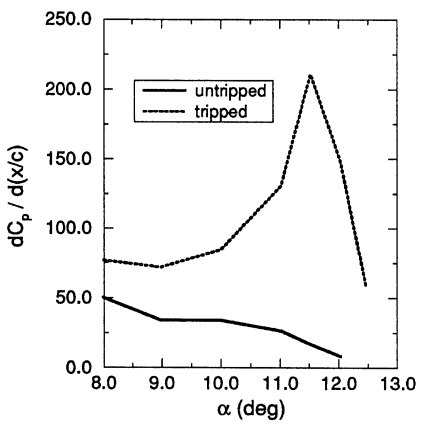

Fig. 5 Adverse pressure gradient development for oscillating 6-in. chord airfoil: $M = 0.35$ and $k = 0.05$.

in a subsonic freestream. These unsteady transonic flow waves can cause dramatic variations in pressure along the weak shear layer enclosing the bubble, which could either alter the bubble dynamics by influencing transition and reattachment or simply force separation by preventing reattachment, causing dynamic stall, depending on their instantaneous strength. If the bubble continues to exist, its bursting is dictated by the pressure distribution in the supersonic flow unlike that seen for the lower freestream Mach number case where the flow was subsonic everywhere. Whereas dynamic stall eventually ensues, these are fine-scale events that compete with each other and play a major role in dynamic stall onset. Further, it is very difficult to capture these details experimentally. But the effects are easily discernible once stall has begun. In Fig. 4d, at $\alpha = 12.03$ deg, the shear layer at the downstream end of the bubble can be seen to be lifting off the surface as the dynamic stall vortex forms underneath it. Even though shocks are still seen in the flow after the dynamic stall process has begun, flow separation was not attributed to these, because a fringe count indicated that the maximum local

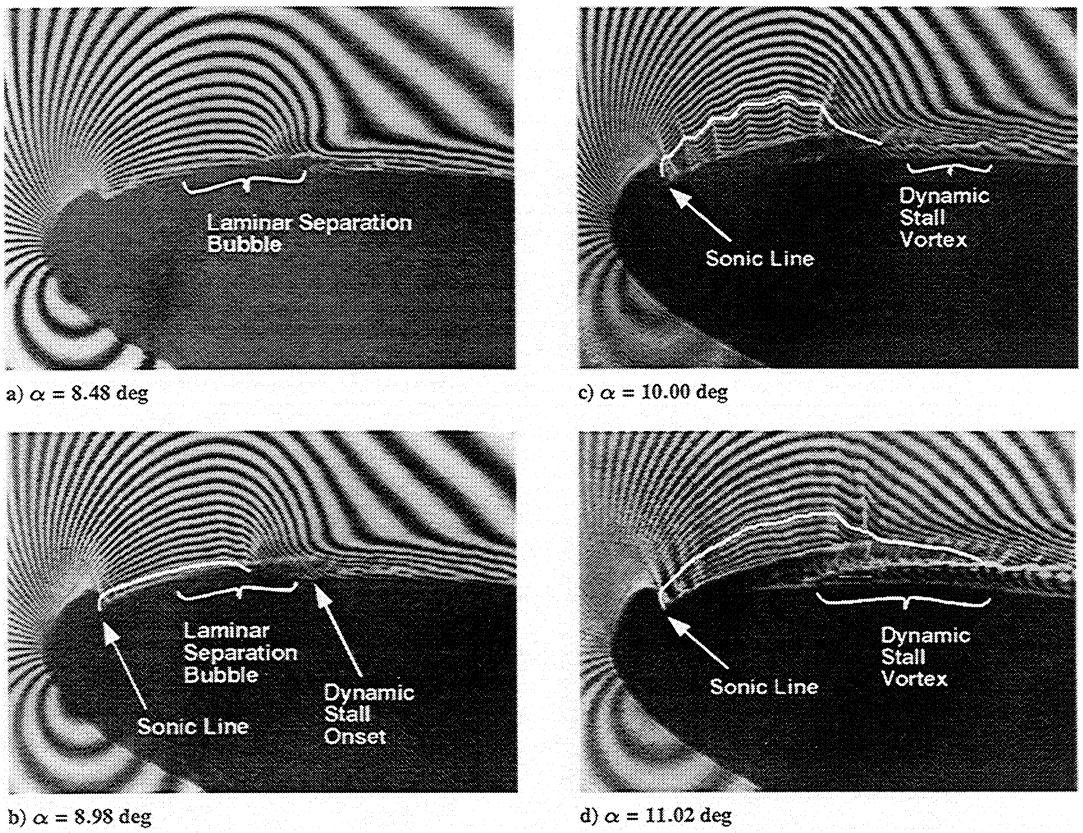

a) α = 8.48 deg
c) α = 10.00 deg
b) α = 8.98 deg
d) α = 11.02 deg

Fig. 6 PDI images illustrating dynamic stall onset from interactions of laminar bubble and locally supersonic flow at M = 0.45 and k = 0.05 for the untripped 3-in. chord airfoil.

Mach number upstream of the shock was only about 1.1 (Ref. 4). Interestingly, the airfoil peak suction increases slightly during further pitch-up of the airfoil. This is because dynamic stall begins at $x/c \approx 0.035$, and until the upstream end of the vortex reaches the leading edge, the peak suction development continues, because there is no propagation of information upstream (except through the separated shear layer) in the local supersonic potential flow. Although a similar result was obtained at $M = 0.3$, the supersonic flow for the case of $M = 0.35$ resulted in a much altered viscous/inviscid interaction.

The distributions of the adverse pressure gradient in the untripped and tripped flow at $M = 0.35$ and $k = 0.05$ (obtained using the same procedure used for Fig. 3) are shown in Fig. 5. A dramatic difference can be seen between the two. As stated earlier, the development of the fringes parallel to the airfoil surface after the suction peak results in very low adverse gradients. Yet, dynamic stall occurred by about 11.5 deg. In contrast, if the same airfoil was properly tripped, a very large adverse pressure gradient develops before dynamic stall occurs. Thus, Figs. 4 and 5 clearly illustrate the very different mechanisms of dynamic stall that can occur depending upon changes in local flow conditions.

Figure 6 shows a similar sequence of events as described earlier, but for $M = 0.45$ and $k = 0.05$ for the 3-in. untripped airfoil. The higher freestream Mach number means that supersonic velocity is reached at even lower angles of attack, where the bubble is still not subjected to the large adverse pressure gradient. The spread of the supersonic region is more rapid in this case due to the higher initial Mach number, and thus the range of angles of attack over which the interactions described earlier occur is smaller, leading to an even earlier dynamic stall onset (by about 9.5 deg). The qualitative similarity between the results presented at the two different Reynolds numbers in Fig. 4 ($Re = 1.3 \times 10^6$) and Fig. 6 ($Re = 0.81 \times 10^6$) confirms that compressibility effects drive the major flow events. It is noted that at the same freestream Mach number the higher-Reynolds-number flow produces a larger suction peak value and, thus, a higher local Mach number. Thus, Reynolds number affects the physics of the problem through the significantly altered viscous/inviscid interactions that are responsible for the development of peak suction, which primarily determines the strength of the supersonic flow and the state of the boundary layer, which in turn determines whether a bubble forms, etc.

These cases provide examples of the situation in which the dynamic stall process could have been caused by the bursting of the bubble if the supersonic flow had not interfered with the shear layer and the bubble, creating competing mechanisms of stall onset. If the local Mach number were slightly higher, shock-induced separation would have occurred as will be shown in the next section.

D. Shock-Induced Dynamic Stall

The interferograms presented in Fig. 7 for the 6-in. untripped airfoil at $M = 0.45$ and $k = 0.05$ show several interesting features. In Fig. 7a, $\alpha = 7.53$ deg, there is a laminar separation bubble. But the velocity at the suction peak is supersonic as can be inferred from a fringe count (see Fig. 1). However, the bubble is still in the subsonic region. Figure 7b shows an increase in the extent of the supersonic region as the angle of attack increases to 7.97 deg, but it is still far from the end of the bubble. By the time the airfoil pitches to 8.40 deg (Fig. 7c), the bubble is enclosed by the supersonic flow. The bubble must respond to this change in the external flow, and any further developments in the bubble now occur under this supersonic external boundary condition. Interestingly, no flow separation can be seen, unlike that observed in Fig. 5. As before, some expansion and compression waves are now seen under the sonic line. The largest of these is close to the end of the bubble. With a slight increase in angle of attack, the last of these waves becomes a shock as can be seen in Fig. 7d at $\alpha = 9.0$ deg. This can be seen more clearly in Fig. 7e, in which the fringes converge toward the foot of the shock from the vertical direction. This distinguishes the fringe pattern for the shock from that of the bubble where the fringes occupy a finite spatial extent along the airfoil upper surface. The shear layer thickens significantly and lifts off the surface from under the foot of the shock. A dramatic change in the boundary-layer thickness can be seen across the shock as well. This signals the onset of dynamic stall for this flow condition. A fringe count in this image shows that the Mach number at the foot of the shock exceeds 1.2, and thus the pressure rise across the shock is large enough to induce

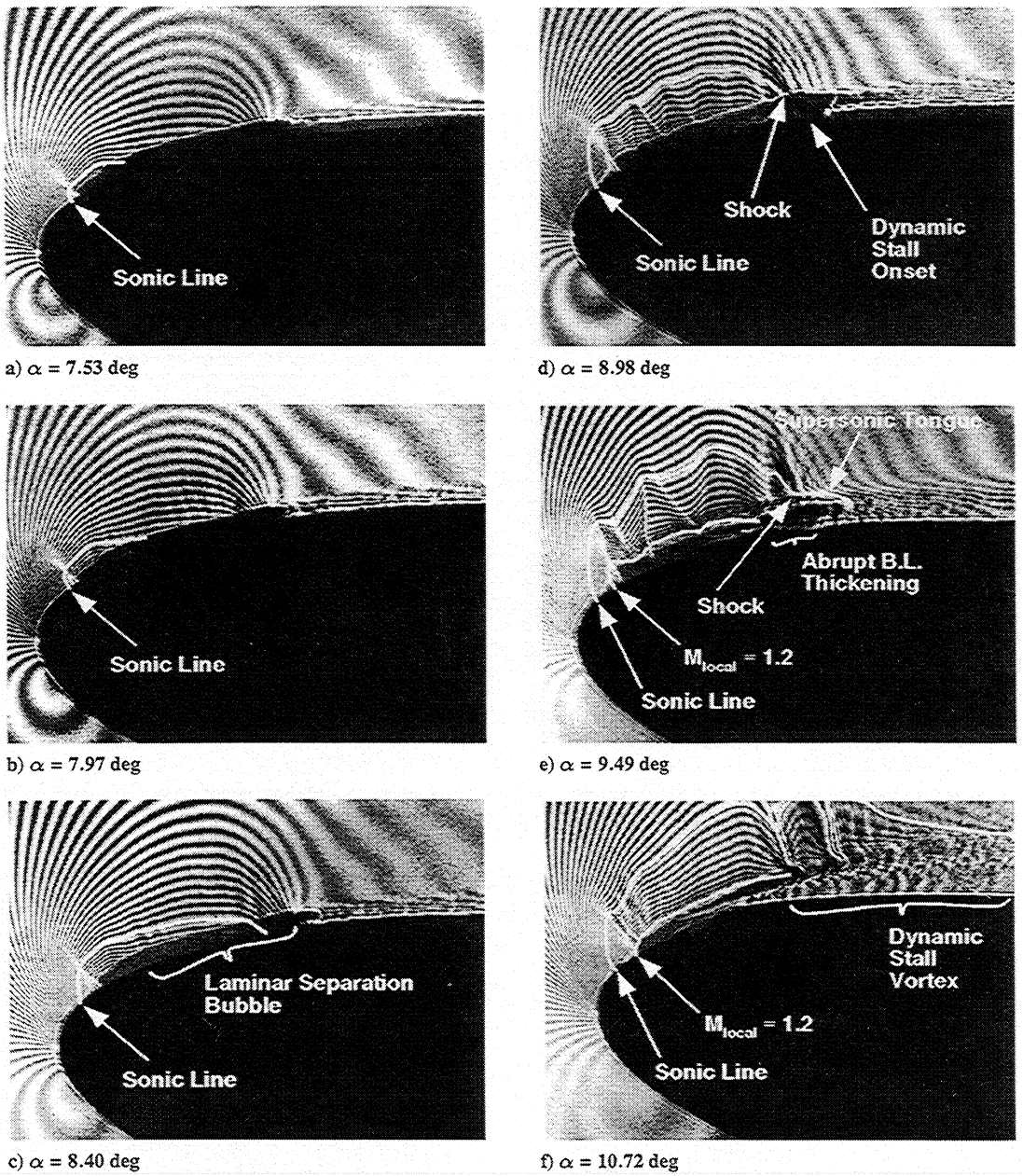

Fig. 7 PDI images illustrating shock-induced dynamic stall at $M = 0.45$ and $k = 0.05$ for the untripped 6-in. chord airfoil.

boundary-layer separation. A tracing of the fringe corresponding to $M_{\text{local}} = 1$ shows that a supersonic tongue extends in the downstream direction and the dynamic stall process and vortex now have to develop under this new external flow condition. This is very much different from the picture in the subsonic case where once the dynamic stall vortex forms, it grows quickly and pushes the external flow outwards, dramatically increasing the transverse length scale in the flow. At low speed, the vortex is indeed circular, whereas, in the compressible case, its imprint is oval in shape, being constrained by the outer supersonic flow. At $\alpha = 9.49$ deg (Fig. 7e), the dynamic stall onset point has moved farther upstream as the shear layer enveloping it moves outward. The multiple shock pattern is now clear in the picture. In fact, the beginning of each wave from the tip or foot of the preceding wave supports the claim that these are caused by wave reflections as already described. At an angle of attack of 10.72 deg (Fig. 7f), the oblong dynamic stall vortex has extended to about 25% chord point. But, strong multiple shocks are still present above the shear layer enveloping the vortex. The supersonic flow and tongue have a strong influence on dynamic stall development. The evolution and behavior of the dynamic stall process under such strongly compressible conditions and the persistence of dynamic lift will depend on this influence. It can be expected that the stream tube containing the sonic line converges as the vortex grows, causing the flow to decelerate because decrease in area results in decrease in velocity in supersonic flow. The leading-edge suction also drops as the separation point moves to the leading edge. Eventually, the velocity becomes subsonic as the flow negotiates the adverse pressure gradient farther downstream along the airfoil. The vortex could then grow in the manner it would in subsonic flow. Depending on when this pressure disturbance reaches the trailing edge, the circulation and hence lift, drag, and moment are affected further. Some of the details of the flow provided here are similar to those described by Osborne and Pearcey.[13] However, much of the latter relates to steady flow and a shock-induced separation bubble, unlike the present unsteady flow situation where a laminar separation bubble was initially present but was subsequently overwhelmed by the supersonic flow above it.

When the airfoil was tripped, the bubble, of course, was not present. For this case, the supersonic region above the airfoil was comparable to the untripped case, but it had a long tail along the airfoil upper surface. The PDI pictures clearly showed dynamic stall to originate from the foot of the last strong shock. All other details were found to be qualitatively similar. The supersonic tongue and the oblong dynamic stall vortex were still seen.

IV. Conclusions

1) This study shows that compressible dynamic stall is influenced by three different, competing factors at low and moderate Reynolds numbers.

a) Dynamic stall is caused by the bursting of the laminar separation bubble at low Reynolds numbers and moderate Mach numbers.

b) As the Mach number is increased, the interaction between the supersonic flow and the bubble can initiate the dynamic stall process.

c) At still higher Mach numbers, shock-induced boundary-layer separation is the cause of dynamic stall. The dynamic stall flow and vortex evolve under a supersonic external flow.

2) Depending on local flow conditions, the fluid dynamic interactions vary, thus strongly influencing the dynamic stall onset process.

3) All of these aspects need to be modeled properly if attempts to compute the flow are to be successful.

Acknowledgments

The project was supported by ARO-MIPR-96-7 to the U.S. Naval Postgraduate School and was monitored by T. L. Doligalski. The work was carried out in the Fluid Mechanics Laboratory Branch of NASA Ames Research Center. The support and encouragement of the branch chief, S. S. Davis, and the help of R. A. Miller in model installation are greatly appreciated.

References

[1]Carr, L. W., Chandrasekhara, M. S., and Brock, N., "A Quantitative Study of Unsteady Compressible Flow on an Oscillating Airfoil," *Journal of Aircraft*, Vol. 31, No. 4, 1994, pp. 892–898.

[2]Wilder, M. C., Chandrasekhara, M. S., and Carr, L. W., "Transition Effects on Compressible Dynamic Stall of Transiently Pitching Airfoils," AIAA Paper 93-2978, July 1993.

[3]Chandrasekhara, M. S., and Carr, L. W., "Compressibility Effects on Dynamic Stall of Oscillating Airfoils," *Aerodynamics and Aeroacoustics of Rotorcraft*, AGARD-CP-552, 1995, pp. 3.1–3.15.

[4]Pearcey, H. H., "Some Effects of Shock-Induced Separation of Turbulent Boundary-Layers in Transonic Flow Past Airfoils," *Boundary Layer Effects in Aerodynamics*, Her Majesty's Stationery Office, London, 1955, Chap. 9.

[5]Chandrasekhara, M. S., Wilder, M. C., and Carr, L. W., "Boundary Layer Tripping Studies of Compressible Dynamic Stall," *AIAA Journal*, Vol. 34, No. 1, 1996, pp. 96–103.

[6]Sankar, L. N., and Tassa, Y., "Compressibility Effects on Dynamic Stall of a NACA 0012 Airfoil," *AIAA Journal*, Vol. 19, No. 5, 1981, pp. 557–568.

[7]Choudhuri, P. G., and Knight, D. D., "Effect of Compressibility, Pitch Rate, and Reynolds Number on Unsteady Incipient Boundary Layer Separation," AIAA Paper 95-0782, Jan. 1995.

[8]Chandrasekhara, M. S., Wilder, M. C., and Carr, L. W., "Reynolds Number Influence on 2-D Compressible Dynamic Stall," AIAA Paper 96-0073, Jan. 1996.

[9]McCroskey, W. J., McAlister, K. W., Carr, L. W., and Pucci, S. L., "An Experimental Study of Dynamic Stall on Advanced Airfoil Sections, Vol. 2: Pressure and Force Data," NASA TM-84245, July 1982.

[10]Carr, L. W., and Chandrasekhara, M. S., "Design and Development of a Compressible Dynamic Stall Facility," *Journal of Aircraft*, Vol. 29, No. 3, 1992, pp. 314–318.

[11]McAlister, K. W., and Takahashi, R. K., "NACA 0015 Wing Pressure and Trailing Vortex Measurements," NASA TP-3151, AVSCOM TR-91-A-003, U.S. Army Aeroflight Dynamics Directorate, Moffett Field, CA, Nov. 1991.

[12]Guderley, G., "On the Presence of Shocks in Mixed Subsonic-Supersonic Flow Patterns," *Advances in Applied Mechanics*, Vol. 3, Academic, New York, 1953, pp. 145–184.

[13]Osborne, J., and Pearcey, H. H., "A Type of Stall with Leading-Edge Transonic Flow and Rear Separation," *Facilities and Techniques for Aerodynamic Testing at Transonic Speeds and High Reynolds Numbers*, AGARD-CP-83-71, 1971, pp. 4.1–4.11.

R. W. Wlezien
Associate Editor